

Continuous and Burst-like Accretion onto Substellar Companions in Mira Winds

Curtis Struck¹*, Babak E. Cahanim²* and Lee Anne Willson¹*

¹*Dept. of Physics and Astronomy, Iowa State University, Ames, IA 50014 USA*

²*Center for Space Research, M.I.T., Cambridge, MA 02139 USA*

29 October 2018

ABSTRACT

We present numerical hydrodynamical modeling of the effects of a giant planet or brown dwarf companion orbiting within the extended atmosphere and wind formation zone of an approximately solar-mass Mira variable star. The large-scale, time-dependent accretion flows within the radially oscillating and outflowing circumstellar gas around Miras are related to Bondi-Hoyle-Lyttleton flows, but have not, to our knowledge, been previously modelled. The new models presented in this paper illustrate the changes in accretion and wake dynamics as the companion mass is varied over a range from 10 to 50 Jupiter masses (M_J), and generalize the results of the single model we presented in an earlier paper.

The character of the accretion onto the companion changes greatly as the companion mass is increased. At the lowest companion masses considered here, a low continuous rate of mass accretion is punctuated by large, nearly periodic bursts of accretion. When the companion mass is large, the mass accretion has both a continuous part, and a rapidly varying, nearly stochastic part. Surprisingly, the angular momentum of the accreted gas shows an opposite trend with mass, varying nearly periodically at large companion masses, and stochastically at low masses. These trends can be understood as the result of the interplay between the shocks and radial oscillations in the circumstellar gas, and the wake flow behind the companion. Boundary conditions also affect the character of the accretion. The equation of state, however, is found to have little effect, at least for gamma-law gases, with gamma in the range from 1 to 5/3.

Models with accretion bursts may produce observable optical brightenings, and may affect SiO maser emission, as we suggested in previous papers. Interruptions of continuous accretion, or shadowing effects, could give rise to bursts of dimming in the optical. Such dimming effects are likely to be correlated with bursts and optical flashes, helping to explain some rather mysterious Hipparcos observations.

Key words:

stars: variables: stars – AGB and Post-AGB – accretion, accretion discs – masers – circumstellar matter – planetary systems: stars – winds.

1 INTRODUCTION

The number of known extrasolar planets orbiting nearby stars is now more than 100 (see e.g., the website: <http://exoplanets.org>). Because of strong observational selection effects most of the systems discovered first consisted of a Jovian planet in a very close orbit around the parent star. Multiple planet systems have been discovered now, as have

systems with Jovian planets or low mass brown dwarfs with orbital radii more like those of our own solar system.

The question of how these diverse solar systems formed has generated much interest. As in our own solar system, there are also many interesting questions about the fate of these systems when their parent stars reach the end of their evolution. However, it is difficult to discover planets around luminous, bloated giant stars. Thus, if this study is to advance in the near future, unique and strong observational signatures of planets around evolved stars must be found.

Soker (1996a) and Soker & Rappaport (2000) (also see

* E-mail: curt@iastate (CS); spyder8@mit.edu (BEC); lwillson@iastate.edu (LAW)

Mastrodemos & Morris 1998 and Mastrodemos & Morris 1999) have suggested that the elliptical, bipolar and even non-axisymmetric shapes of planetary nebulae could be the result of their binary nature, with the binary companion being a substellar object in many cases. Soker (1996b) has also proposed that jets in planetary nebulae could be formed as a result of the engulfment of giant planets or brown dwarfs in the envelope of AGB stars. Livio & Soker (2002) recently proposed that such engulfments could modify the mass loss of the AGB star. They estimated that at least 3.5% of solar type stars would be affected. These phenomena provide strong observational signatures, but the disadvantage is that the substellar companion must disappear in most cases (and in a short time) to produce them.

We have suggested that other observable signatures may result from the accretion of AGB wind or extended atmosphere material onto closely orbiting giant planet or brown dwarf companions. These include enhancing SiO maser emission in Mira variables (Struck-Marcell 1988), and producing short time-scale optical variations (Willson & Struck 2001), such as reported in Hipparcos observations of Miras (de Laverny, et al. 1998). Previously (Struck, et al. 2002, henceforth Paper I) we presented some preliminary numerical hydrodynamical models of the accretion process.

These signatures do not require the companion to be swallowed, but the optical variations are more subtle and difficult to detect. The masers, in particular, may have multiple causes, so the role of companions is difficult to decipher. Moreover, the companion masses and radii are restricted by the need to have a strong enough accretion interaction to produce the observable phenomena.

When solar-type stars evolve to the AGB stage, their outer atmospheres expand out to nearly an astronomical unit. During parts of this evolutionary stage they experience radial pulsations as Mira or semi-regular variable stars, suffer thermal pulses, and generate winds that increase with time. The models of Bowen (1988) show how pulsational shocks steepen as they run down the pressure gradient outside the photosphere, ultimately lifting material into an oscillating extended atmosphere. Further out, where gravitational periods are longer, individual gas elements are not able to complete a cycle between shocks, and a wind develops (Hill & Willson 1979). Radiation pressure on dust grains also contributes to driving the wind (e.g., Bowen 1988, Gail & Sedlmayr 1999, Willson 2000). The dominant pulsational modes in Miras are radial, so it is likely that the wind is spherically symmetric, unless the atmosphere has been spun up or otherwise modified by interaction with a close companion. The discovery of concentric shells around some young planetary nebulae provides strong evidence for circular symmetry in the winds (e.g., Balick, et al. 2001 and references therein).

Any companions within the large optical photosphere of the Mira star will be swallowed - that is, heated and dispersed as they are dragged inward. Companions orbiting at distances of greater than about 10 AU from the central star will accrete, but accretion from the quite steady and relatively low-density wind at these radii is unlikely to generate any very strong observational signatures. (That is, unless the companion is of stellar mass, see Mastrodemos & Morris 1998 and Mastrodemos & Morris 1999.)

The best place to produce time-varying observable ef-

fects with accretion onto low-mass companions is closer to the star, where they can interact with pulsational shocks in the extended atmosphere. According to the Bowen (1988) models, pulsational shocks, and quasi-ballistic motions of gas elements with radial velocity sign changes, persist out to radii of about 10AU in typical Miras. In Willson & Struck (2001) and Paper I we found, from energy estimates and preliminary models, that even this close to the central star, it is unlikely that steady accretion onto giant planets and low-mass brown dwarfs would produce observable effects. In this region the pulsational shocks modulate the amount of material that sweeps into the companion's sphere of influence, though not by enough to give rise to large emission bursts.

Captured material has little specific angular momentum relative to the companion, so we expect it to settle into a disc of radius R much less than the capture radius R_{cap} . (For clarity, we will refer to radii or distances from the companion with a capital letter R, and distances from the Mira with the lower case r.) Because the surrounding medium is oscillating in radius, the sign of the accreted angular momentum is expected to change periodically. (As discussed below, the situation is in fact more complicated than this.) Thus, we expect a disc to build up near the companion with the gas orbiting in one sense, but to be disrupted when gas orbiting in the opposite sense begins to rain down. The resulting angular momentum cancellation would drive infall onto the planet, with a burst-like energy release. The transient disc essentially serves as an energy reservoir, allowing substantial burst-like releases. The models presented below do not spatially resolve the accretion disc, but they can provide some information on its development.

We note in passing that, since we are only considering companions that are much less massive than the star, the accretion process is not Roche overflow, but rather direct hydrodynamic capture from the surrounding medium. Similarly, estimates of the tidal circularization or in-spiral time (see Section 2 of Soker 1996a and references therein), show that tidal effects will only be important over the brief Mira lifetime (about 3×10^5 yrs.) if the companion orbits within about $r = 3.0$ stellar radii of the star. The oscillating extended atmosphere extends much farther out than this. The orbital radius adopted in the models below is 3.2 times the radius of a solar mass Mira (e.g., Bowen 1988). (There is controversy in the literature about Mira radii, but larger Mira radii would also imply larger oscillatory zones, and not change the conclusion that tidal effects are only important in the lower part of this zone.)

The bow shock, wake and accretion phenomena in this problem are examples of the Bondi-Hoyle-Lyttleton class of wake accretion flows (Hoyle & Lyttleton 1939, Bondi & Hoyle 1944, Cowie 1977). In the last 20 years there has been a great deal of study of the problem of accretion in X-ray binaries, where a compact object orbits within the wind of a massive star (e.g., Fryxell, Taam, & McMillan 1987, Fryxell & Taam 1988, Taam & Fryxell 1988, 1989, Ho, et al. 1989, Soker 1991, Taam, et al. 1991, Livio, et al. 1991, Ishii, et al. 1993, Ruffert 1994, 1995, 1997, 1999, Ruffert & Arnett 1994, Ruffert & Anzer 1995, Foglizzo & Ruffert 1997, 1999, & Pogorelov, et al. 2000). These flows are very similar to those of the present work - unstable, oscillating wakes and bursty accretion of low angular momentum gas are also common

in them. We will make specific comparisons to this work below. However, we note that because the time-dependent hydrodynamics is driven by “external” pulsational forcing in the present problem, it is fundamentally different than that of the flip-flop internal instability found in models of X-ray binary stars.

In the earlier work we also found that companions must be considerably more massive than Jupiter to produce observable bursts, i.e., at least 10 times as massive. The brown dwarf/planet boundary is usually defined as the critical mass for deuterium burning, about $13 M_J$ (Jupiter masses). In the models below we consider companion masses in the range 10-50 M_J . As the companion mass is increased through this range we find an interesting transition in the wake and accretion hydrodynamics. If we further increase the companion mass much above this, e.g., $M \geq 80 M_J$ the companion would no longer be substellar, and we would be entering the domain of the symbiotic star phenomenon, which is beyond the scope of this paper.

Once we have restricted consideration to systems with brown dwarf companions orbiting within 10 AU of a Mira variable, we must return to the question of how common are such systems? The question is especially important in light of the two points: 1) most of the recently discovered brown dwarfs are young, freely floating in star-forming regions (e.g., Reid, et al. 1999, Lucas & Roche 2000, Zapatero Osorio et al. 2000), and 2) for several years after the discovery of extrasolar planets, it appeared that there was a “brown dwarf desert.” The latter point refers to the fact that as extra-solar planets were being discovered, brown dwarf companions were not found (see review of Marcy & Butler 2000 and references therein).

The difficulty posed by this point has been mitigated recently. Specifically, the first 50 extrasolar planets discovered included only 3 objects with $M_{\text{sin}} \geq 10 M_J$, but all had orbital radii much less than 1AU. However, the second 50 planets discovered include 5 objects of about this mass or somewhat greater, and all have orbital semi-major axes of greater than 1AU. Thus, near the planet/brown dwarf boundary, the desert is less deserted.

Some specific systems are also noteworthy. These include the HR 7672 (HD 190406) system, with a solar analog star. The mass of its companion is estimated to be in the range of about $50 - 80 M_J$, and its orbital semi-major axis is about 14 AU (Liu et al. 2002). It provides an example of a high mass brown dwarf companion of a solar type star. The more massive of the two companions in the HD 168443 system has $M_{\text{sin}} = 17.2 M_J$, and a semi-major axis of 2.9 AU (eccentricity of $e = 0.20$) (Marcy et al. 2001), which very much fits the range of this study. ι Draconis (HD 137759) is a roughly solar mass K giant star with a companion minimum mass of $8.9 M_J$, and whose semi-major axis is about 1.3 AU (eccentricity 0.7, see Frink et al. 2002). This planet, the first discovered orbiting a giant, may be doomed when the parent reaches the AGB stage.

These examples show that while systems with closely orbiting brown dwarf companions may be quite rare, they do exist. In the following sections we investigate the accretion hydrodynamics they generate at the end of the parent stars’ life, and the consequences for observation.

2 THE NUMERICAL MODELS

The models were produced with a smoothed particle hydrodynamics code, which is described in Paper I, and Struck (1997). Since the code is documented in these papers, here we will only describe the initial conditions, boundary conditions, and scaling issues relevant to the present models.

First of all, the gravities of the parent star and companion were approximated as softened point masses. The SPH smoothing length in these models was fixed in space and time to a value of 0.1 length units. The unit of length is taken to be 1.0 AU, and the time unit is 1.0 yr. The gravitational softening length of the companion was set to 0.08 length units.

Most of the runs described below used 157,500 gas particles distributed in a complete (360°) annulus in the orbital plane of the companion. Initially, the particles were placed on a circular grid with constant radial separations between particle circles. A fixed number of particles were placed on each circle, since this gives a $1/r$ density profile in two dimensions, which is like the observed $1/r^2$ profile in three dimensions. The particles were also given a slight random offset from this grid, and a small random velocity (5 of the sound speed in each of the 2 dimensions), to produce a smooth distribution. Particle radial and azimuthal velocities were initialized to zero, except for the random part. The parent simulation code is three dimensional, but the present simulations are two dimensional.

In the model presented in Paper I, an isothermal equation of state was used with an initial temperature of $T \simeq 1700 K$. The simulations described below also used a polytropic or gamma law equation of state, $P \propto \rho^\gamma$. Runs with different values of γ were carried out to test the effects of this factor. The Mira atmosphere and wind models of Bowen (1988) show that the presence of a small amount of dust can so enhance the cooling behind the pulsational shocks that the extended atmosphere is nearly isothermal. However, Bowen models with no dust show large temperature variations. Thus, the isothermal case may be the most relevant, but is not the only case of interest.

The first boundary condition, for the inner boundary, is a wall that is moved inward and outward on a cycloidal trajectory, like that of a ballistic particle at the same distance from the star. The radial range of this motion is from $r = 2.0$ to about 2.5 AU, and its period is about one time unit.

As in the model of Paper I, we neglect the effect of radiation pressure on grains. Then, as noted in that paper, pulsational waves generated from below with the piston-like boundary, and a zero pressure outer bound, reproduce the main features of the flow in Bowen’s (dust-free) models, including, approximately, the velocity profile.

In the model of Paper I the outer boundary was an impervious, reflecting wall, that was moved steadily outward. This motion avoided reflection shocks from the outer boundary, and was responsible for the low pressure that allowed the development of a wind at larger radii. However, since a fixed number of particles were used, the gas density steadily decreased, so that the model could not be run for a long time.

In the models presented below we used a fixed outer boundary. When gas particles reached this outer bound they were removed from the grid and reinserted just above the

lower boundary, at the same azimuth, and then moved by a small random displacement to smooth any clumps. Their velocities were reset to values close to that of the inner piston. Shock reflections were generally small with this boundary procedure. The procedure does not, however, completely smooth large density changes (e.g., behind shocks), so there will be some feedback effects. No growing instabilities resulted from this feedback, but the gas behind the pulsational shocks did acquire a more complex, multi-layered appearance. Since the companion was only followed through one orbit, the bow shock was not affected.

The final boundary condition is applied on a circle of radius $R = 0.05$ AU (106 Jupiter radii) around the companion. Large numbers of particles are captured by the companion. As noted in the Introduction, the particles have quite small values of specific angular momentum relative to the companion, so we expect them to fall into a very small region around the companion. This region cannot be resolved by the present code, so their fate is determined by the boundary condition. In the model of Paper I they were transferred to the centre of the region, assigned the same velocity as the companion, and thenceforth traveled as a single clump with the planet. We will call this case the clump condition.

In the models presented below, particles found within the boundary radius are removed, and reinjected into the simulation at the lower boundary, just like those passing through the outer boundary. We call this the vacuum condition.

When the clump condition is used the particles in the clump still exert a hydrodynamic pressure on particles outside the boundary, computed according to the usual SPH algorithm. In the Paper I model this pressure was initially small, but grew in magnitude as the clump grew. Eventually, this pressure resisted accretion, and particles accumulated on the circular boundary until their pressure and gravitational force overwhelmed the resistance. This effect was responsible for the burst-like accretion described in that paper. There is no pressure resistance when the vacuum condition is used, and any burst-like accretion must be due to other causes, see below.

In reality, pressure on the outer accretion flow from a small accretion disc is not realistic. On the other hand, such resistance might be generated by other means. For example, if the companion has a strong magnetic field, the magnetosphere would provide magnetic pressure against the partially ionized accretion flow. Energy release from accretion onto the companion surface may generate a hot corona, and coronal pressure around the companion. The clump condition crudely represents such effects (for a limited duration). However, the vacuum condition is more realistic on the relatively large scales modeled here, and ultimately resisting pressures should be modeled on the smaller scales where they are generated.

3 MODEL RESULTS

3.1 Basic Hydrodynamics

We begin each of our model runs with the companion starting on a counterclockwise orbit from a position near the x-axis, and thus, moving through the first quadrant. In a

very short time compared to the orbital period the companion draws gas particles around it into mildly supersonic motion with it. A classic Bondi-Hoyle-Lyttleton bow shock and wake structure soon develop (Hoyle & Lyttleton 1939, Bondi & Hoyle 1944). Figure 1 shows six snapshots through the course of one Mira pulsation cycle (also see Fig. 1 of Paper I), at a time when the companion has moved into the second quadrant. Particles in the wake and the (incomplete) bow shocks are highlighted in the insets, which show magnified views of the region near the companion, and in which only particles with supersonic (i.e., greater than 1.0 velocity units) azimuthal velocities are plotted. Initially the gas particles have zero azimuthal velocities and only acquire them through interaction with the companion. The wakes are truncated at the outer boundary, but can clearly be seen for a length of more than an AU.

Also at the beginning of a model run, the piston at the lower boundary of the annular grid is started outward. As this and subsequent pulsational shocks move radially out through the grid they set up a pattern of radial motions much like those seen in the Bowen (1988) atmospheric models. We model a minimal radial range needed to capture this basic kinematics, in contrast to Bowen's models. The snapshots in Figure 1 show the progress of one shock from the lower piston to the outer boundary.

Recycling material at outer boundary back to the inner boundary does not seem affect the flow much in regions away from the companion. Flow profiles are quite similar to those of Paper I, where a moving/reflecting boundary was used. This is probably because the pulsational shocks are weak by the time they reach this bound in both cases. Nonetheless, the shocks driven by the lower piston do acquire some additional structure from the remnant waves reinserted, but with some smoothing, from the outer bound, as can be seen in Figure 1. Note that a layer of particles "stick" to the lower boundary (a well known effect in SPH). We inject the recycled particles just above this layer.

It is clear from the Figure 1 snapshots and their associated insets that the radial shocks are able to move the companion wake. This is reasonable since the wake column density along a radial line is of the same order as that of the gas immediately behind a pulsational shock. The wake is stretched outward when pulsational shocks sweep over it. The infall in the postshock rarefaction wave leads to reformation of the wake, and leaves it pointing in a slightly inward direction. It is also apparent from Figure 1 that the wake interaction disturbs the pulsation shock and postshock flow. This is especially apparent in the fourth and fifth snapshots of Figure 1, where the shock is disturbed over a distance of nearly 2.0 AU behind the companion.

3.2 Mean Accretion Properties

In this section we consider the mean properties of the accretion flow onto the companion, in the next section we consider its more detailed structure. This accretion is characterized by two radial scales: an accretion radius (and BHL accretion cylinder) from which it is gravitationally captured, and an inner scale equal to the radius of the accretion disc around the planet, where the material settles. As noted above and in Paper I our models do not resolve the inner scale. This means that we cannot account for the possibility that some

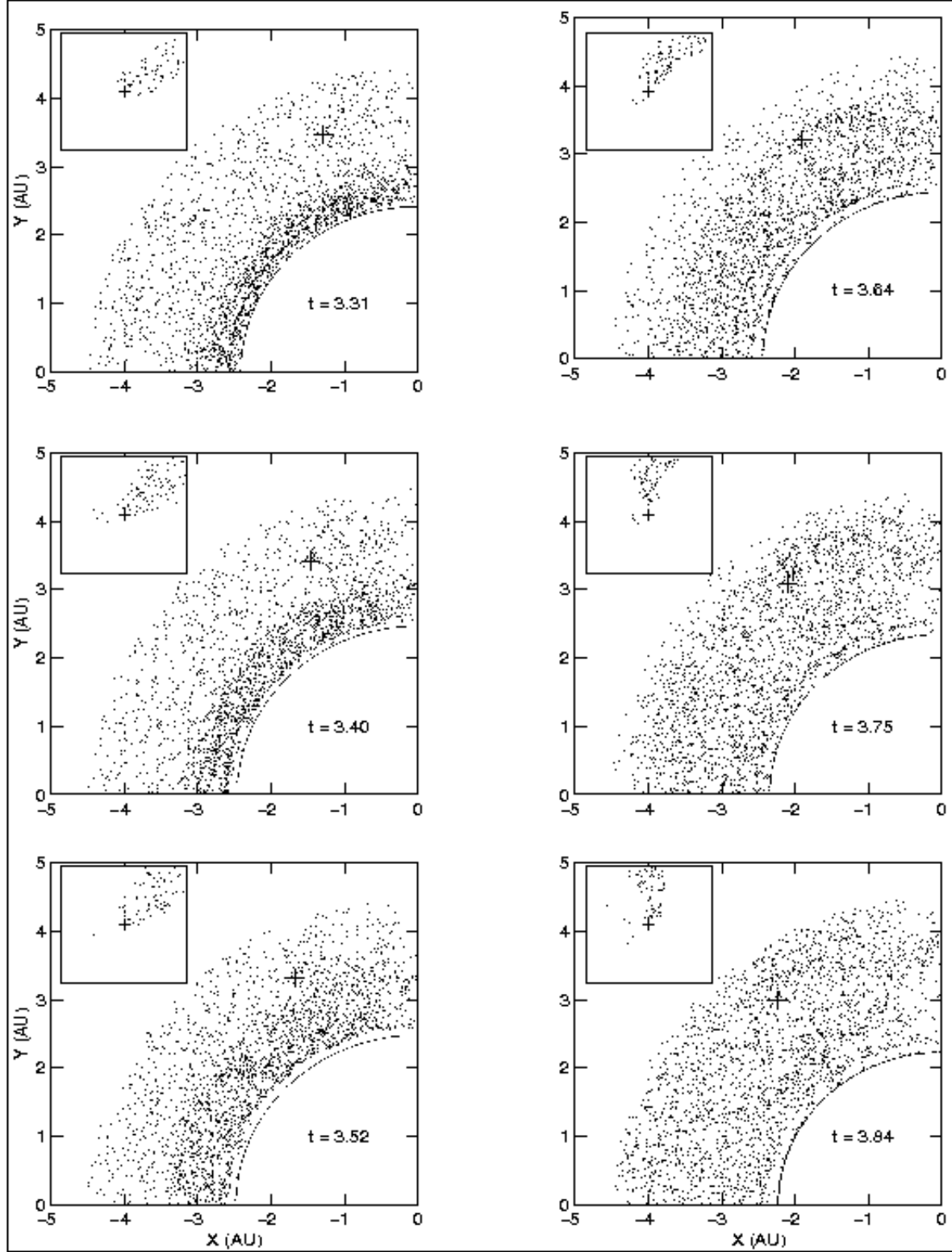


Figure 1. Wind particle positions in the $30 M_J$ model at six timesteps, chosen to cover most of one pulsation cycle. Only a quarter of the computational grid, the quadrant containing the companion at these times, is shown. The Mira star is centred at the origin. The planet's position is marked by a cross in each panel. The size of the inset is $0.35 AU \times 0.35 AU$ in all panels. In the insets the wake is highlighted by plotting only particles with significant velocities greater than the sound speed (see text for details).

captured material may be subsequently pushed back out by dynamical processes at the inner scale, before being accreted onto the companion. However, we expect this to be a small fraction of the captured gas.

In the simulation code, any particle that comes within a radius of $R_{cap} = 0.05$ AU of the companion is assumed to be accreted, and is removed and recycled. Figure 2 shows this estimate of the number of particles captured versus time in five model runs with companion masses of 10, 20, 30, 40 and 50 M_J . The classical BHL accretion radius is,

$$R_{BHL} = \frac{2GM_c}{v_{rel}^2 + c^2}, \quad (1)$$

where M_c is the companion mass, c is the sound speed in the ambient gas, and v_{rel} is the relative velocity of the companion and the ambient gas, i.e., the sum of the companion's orbital velocity and the current ambient radial velocity (see e.g., Shapiro & Teukolsky 1983). (Note that the latter velocity is constantly changing in direction and magnitude, so that the concept of an upstream accretion cylinder out of which gas is accreted becomes somewhat confused.) The adopted value of R_{cap} is about equal to R_{BHL} in the $M_c = 10M_J$ case, and smaller than R_{BHL} for larger companion masses. (In the limit that the relative velocity equals the companion orbital velocity,

$$\frac{R_{BHL}}{a} = 0.019 \frac{M_c}{10M_J} \frac{1.0M_\odot}{M_*}, \quad (2)$$

where a is the companion orbital radius, and M_* the Mira mass.) Thus, the bow shock and accretion cylinder is resolved only for the larger mass companions.

The cumulative accretion in each of the models plotted in Figure 2 is roughly linear with time. In that figure each curve derived from the model data is paired with a line derived from a least squares fit. The deviations between the model data and the fitted line are small in all cases, though interesting as we will see in the next subsection. This implies that the accretion is on average constant, despite the radial pulsations in the extended atmosphere.

Figure 3 compares the accretion rates of the different models. Specifically, it shows the average accretion rate over the duration of each run, plotted against the mass of the companion. In addition to the data points a line fit is shown. This line simply connects the best-resolved 50 M_J case to the origin, since we demand zero accretion for a zero mass companion. Most of the other models lie close to this line except for the poorly resolved 10 M_J model.

As in the classic BHL problem most of the accretion in the more massive companions comes through the wake. In the BHL problem the accretion radius increases with the companion mass, and the accretion rate should increase with the square of this radius. That is, with the square of the companion mass. The goodness of the linear fit in Figure 3 appears to represent the two-dimensional BHL result.

However, in this problem, the near linear fit may be more generally applicable. The oscillatory motions of the ambient gas deliver material to the companion from a greater range of radial distances than $2R_{BHL}$. The companion effectively has a greater reach in the radial direction, though this "reach" still seems to scale with the companion mass. The increase of the size of the accretion cylinder

in the direction perpendicular to the orbital plane with increasing mass (i.e., the increase in R_{BHL}) is smaller and contributes less to the accretion increase than the increase in the radial direction. If this is correct, then in three dimensions, the accretion rate will continue to scale more linearly than quadratically with mass through the brown dwarf mass range. High resolution, three-dimensional simulations are needed to resolve this question.

It is also of interest to compare the numerical mass accretion rates to BHL rates. E.g., the mean mass accretion rate for a 30 M_J companion is about 1500 *particles per yr*, though we will see below that burst rates can be much higher. If we adopt a value for the particle mass of $m_p = 2.0 \times 10^{21}$ g, as in paper I (adjusted for the different particle numbers used here, and assuming a vertical capture distance of $R_{BHL} \simeq 0.2$ AU), then we get the following conversions:

$$1500 \text{ particles per yr} = 9.8 \times 10^{16} \text{ g/s} = 1.5 \times 10^{-9} M_\odot/\text{yr}.$$

The stellar mass loss rate is assumed to be of order $2 \times 10^{-7} M_\odot/\text{yr}$. (This is the mass loss rate of the standard dust-free model of Bowen (1988), and that used in Humphreys et al. (2002), though it is about an order of magnitude less than the typical Mira mass loss rate.) If we compute the Bondi rate,

$$\dot{M} = 4\pi\tilde{\lambda}(GM_c)^2(v_{rel}^2 + c^2)^{-1.5} \rho, \quad (3)$$

using the average circumstellar gas density $\rho = 2.0 \times 10^{-15} \text{ g/cm}^3$, an efficiency of $\tilde{\lambda} = 1.0$, the sound speed at the companion's radius ($c \simeq 3.3 \text{ km/s}$), and set the relative velocity of the companion equal to its orbital velocity we get $\dot{M} = 1.6 \times 10^{-9} M_\odot/\text{yr}$. Thus, the numerical rate nearly equals the Bondi rate. This seems somewhat high, yet it is comparable to those Benensohn, Lamb, & Taam (1997) and Ruffert & Anzer (1995). However, if the BHL scaling with mass does not hold in three-dimensions, then accretion rates in this problem will be very different than BHL rates at the extremes of the brown dwarf mass range.

Finally, we note that the 30 M_J run was repeated with several different values of γ , the exponent in the equation of state. We found hardly any change in the accretion rate as γ was varied. The analytic interpolation formula of Foglizzo & Ruffert (1997) also shows little deviation from the BHL accretion rates at Mach numbers greater than a few, when γ is varied from 4/3 to 5/3. Numerical studies of the flip-flop instability indicate that there is no instability at $\gamma = 1.0$, so the accretion is steady (see Ruffert 1999, Sec. 3.2). This contrasts greatly with the present externally driven case.

3.3 Time-Dependent Accretion

In this section we consider time-dependent aspects of the accretion more carefully. We begin with Figure 4, which shows the instantaneous accretion rate ($\Delta M/\Delta t$) in three of the models. We note the presence of sharp, high amplitude peaks in the accretion rate. There are also sharp decreases relative to the small, but nonzero, mean accretion rate. In all cases the accretion bursts are clustered. The cumulative effect of these clusters is presumably responsible for the deviation from the mean lines in the curves of Figure 2.

A second feature of Figure 4 is the fact that the burst

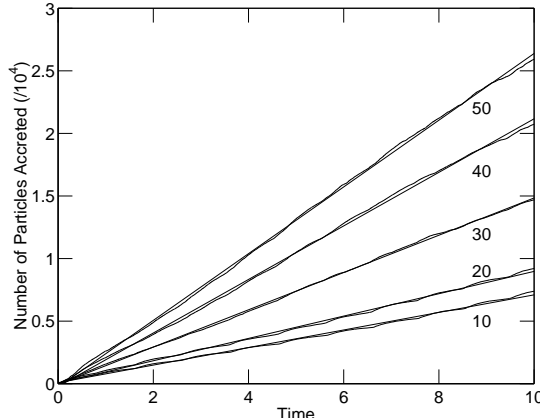


Figure 2. Cumulative number of particles accreted versus time for the $10, 20, 30, 40$, and $50 M_J$ models (labelled). The time unit is one year, and the y-axis is labelled in units of 10^4 accreted particles. See Sec. 4.1 for an estimate of the particle mass. A least squares mean line is fit to each model curve.

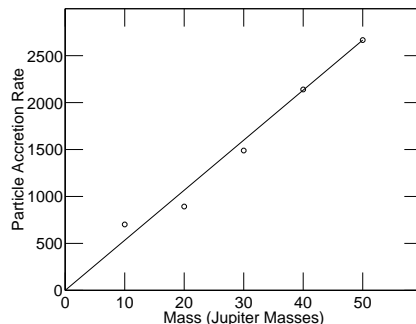


Figure 3. Mean accretion rate versus companion mass for the $10, 20, 30, 40$, and $50 M_J$ models. The values on the y-axis are in units of particles per year, and the derived value for each model is the slope of the line fit to that model shown in Figure 2. The line connects the origin to the $50 M_J$ model, see text for details.

clusters are nearly periodic at low companion mass, but appear to become progressively more random, and frequent, as the companion mass increases. At low masses, the burst period is about equal to the pulsation period, and in fact, the bursts are coincident with pulsational shocks overrunning the companion. It is natural that the companion should accrete more from dense post-shock layers (which is also when the radial velocity changes sign). The bursts are more random with high mass companions because, as we will describe below, of the processing of this material through the longer wake.

Before proceeding we note the similarity of some of these features to those of simulations of flip-flop accretion in X-ray binaries. Instability and quasi-periodic bursts are certainly a characteristic of accretion in this problem as well (e.g., Taam & Fryxell 1988, Fryxell & Taam 1988, Taam & Fryxell 1989, Livio, et al. 1991, Soker 1991, Taam et al. 1991, Ishii, et al. 1993, Ruffert & Anzer 1995, Ruffert 1997, Benensohn, Lamb, & Taam 1997, Ruffert 1999, Pogorelov, et al. 2000). Since the flip-flop instability is self-excited, much of the discussion of this literature has focussed on the question of what circumstances are required for its development. In particular, issues such as the effect of pressure and velocity gradients across the Mach cone have been considered in some detail. Numer-

ical studies have been plagued by spatial size and temporal limitations, as well as numerical resolution problems (see Benensohn, Lamb, & Taam 1997, Pogorelov, et al. 2000, and references therein). The present problem has the advantage of being driven by strong, external perturbations, so we don't have the difficulty of modeling the slow growth of small amplitude perturbations under the internal instability.

As a result of this fundamental difference in the two processes, the details of the accretion burst phenomenon are also different. In the published flip-flop simulations the amplitude of accretion bursts relative to the mean never exceeds a factor of about 5. Figure 4 shows much larger burst amplitudes. There also seems to be no equivalent to the systematic change in the character of the accretion bursts as companion mass is increased, as shown in Figure 4. However, it appears that nonlinear trends with companion (e.g., stellar black hole) mass have not yet been investigated in the flip-flop problem.

We noted above that models with larger mass companions draw gas in from a larger range of radii. Figures 5 and 6 provide many more details about this process for the $10 M_J$ and $50 M_J$ models, respectively. These figures show the partial trajectories of particles that come within a radius of $R_{cut} = 0.075 AU$ of the companion, and their subsequent

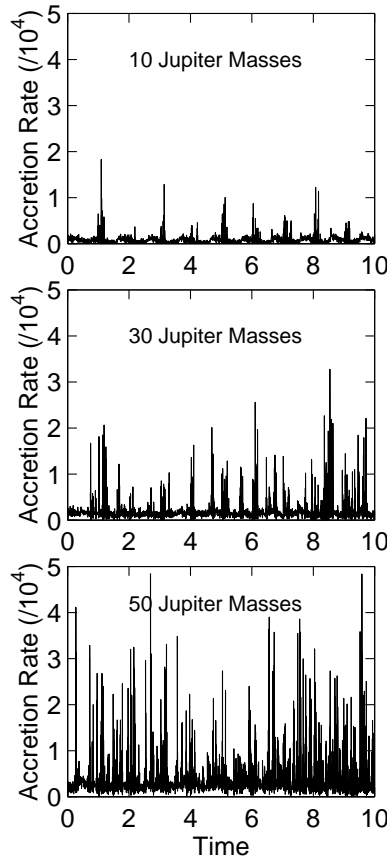


Figure 4. Comparison of the instantaneous particle accretion rate versus time for the 10, 30, and 50 M_J models, with separate panels (labelled) for each model. The y-axis is labelled in units of 10^4 accreted particles.

fate. The value of this cutoff radius is arbitrary, and was chosen to provide an adequate particle sample. Specifically, once the particles within the cutoff radius were identified (at the times indicated), their positions relative to the companion at 4 previous output times were used (with the present position) to produce the curves. Since the companion position is fixed in these plots, the primary component of these trajectories is the relative azimuthal motion toward the companion. (Note: the companion is located in the second quadrant at these times.)

In Figure 5 and the first panel of Figure 6 the time shown is when a pulsational shock is just about to overrun the companion. This is evident in the abrupt trajectory changes visible on the right side of the companion. The second panel of Figure 6 shows a time of about half a pulsational cycle after that of the first panel, when no shock is near the planet. At that time the trajectories are smoother, and more symmetrically distributed.

Figure 6 not only shows that many more particles are drawn in by the 50 M_J companion, but also resolves the capture process quite well. A large fraction of the accreted particles circle around the companion, impact the wake, and are drawn down from the inner wake. The trajectories coming from above (behind in the orbital sense) are especially interesting. Some particles still escape through the outer wake, but they are a much smaller fraction with the 50 M_J companion.

With this information, we can now understand the patterns of instantaneous accretion in the different models. In the low mass models accretion bursts result from enhanced feeding associated with the passage of pulsational shocks. Because gas accretes through a larger wake in the higher mass cases, we would expect longer duration burst clusters. There is also a possibility of echo bursts following passage of a pulsational shock, if relatively large amounts of gas are deposited in the wake, and its accretion is significantly delayed.

The middle panel of Figure 4, for the 30 M_J model, does indeed show wider burst clusters, and bursts appearing at new phases. When the companion mass is increased to 50 M_J the wake becomes so massive that the passage of pulsational shocks does not greatly enhance the accretion. There is still some hint of periodicity in the bursts in the third panel of Figure 4, but the duration of the burst clusters is comparable to the time between them.

To further probe the dependence of the accretion process on companion mass, it is worth looking at the wakes in more detail. Like the insets of Figure 1, Figure 7 shows only those gas particles that have acquired significant azimuthal velocities, though in Figure 7 we show the 5 models at about the same time, rather than snapshots of one model. The wakes are much longer and more massive when the companion mass is large. In fact, in the case of the most massive companions the graphs underestimate the extent of

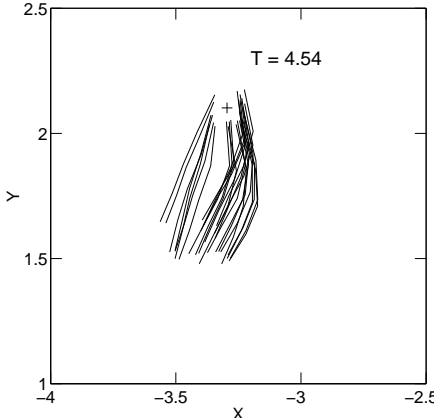


Figure 5. Partial trajectories of 27 accreted particles relative to the fixed companion position (marked with a cross) in the $10 M_J$ model are shown at the time indicated. Part of one quadrant of the simulation volume is shown. The particle trajectories are constructed by choosing particles within a capture radius of 0.075 AU at the given time, and connecting their positions at several previous times with straight line segments.

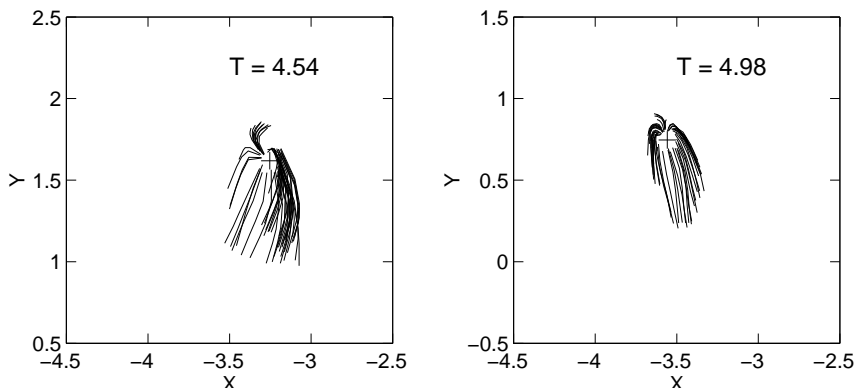


Figure 6. Partial trajectories of about 100 accreted particles as in the previous figure, but from the $50 M_J$ model, and at two timesteps differing by about half a pulsation period.

the wake, because wake particles reach the outer bound and are recycled. We note that the particle clumps seen in the lower centre part of the graphs for $M = 40, 50 M_J$ are apparently bow shock particles that have moved to the outer bound and have been recycled.

Figure 7 also shows us that the bow shock is barely detectable in the low mass cases, and asymmetric in the high mass cases. The phase dependence of this asymmetry can be seen in Figure 1. Gas behind the bow shocks is pushed outward, like wake gas, by the passage of pulsation shocks. Following these passages, material sweeping past the inner side of the companion encounters little resistance. Material moving forward toward the outer side of the companion impacts both bow shock and wake.

3.4 Accreted Angular Momentum

In Paper I we suggested that the angular momentum vector, relative to the companion, of material accreted out of the radially oscillating circumstellar gas would change signs with pulsation phase. Figure 8 shows the mean specific angular momentum of the accreted gas as a function of time in the $10, 30$, and $50 M_J$ models. This figure confirms the fact that

the accreted angular momentum does have both positive and negative signs at different times, though the positive (counterclockwise) sign seems predominant. Moreover, the sign changes are often quite rapid.

What is even more striking about Figure 8 is the contrast with Figure 4. It appears that the values of accreted angular momentum are quite random at low companion mass, where the mass accretion is periodic, and the angular momentum accretion is periodic at high companion mass, where the mass accretion is much less regular. A somewhat more careful reading is that at low mass the amount of accreted angular momentum is just low. Evidently, even with the passage of pulsational shocks, gas is accreted relatively symmetrically in the low mass case, with little net angular momentum. Some of this effect may be due to low resolution of asymmetries in the low mass case. However, the size of the accretion radius is smaller than the thickness of the dense post-shock layer in the low mass case, and more comparable in the high mass case. Thus, density asymmetries are not noticeable on the accretion scale in the low mass case, but are in the high mass case.

The representative particle velocity vectors shown at two times in Figure 9 provide more detail on the wake hy-

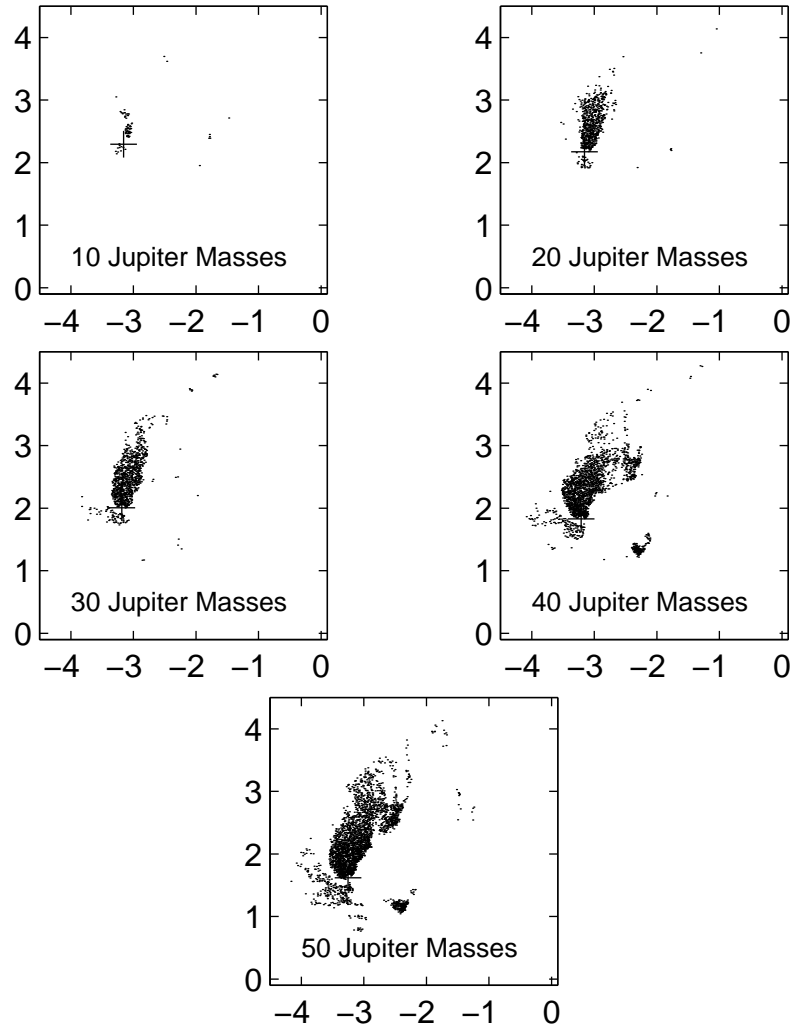


Figure 7. Positions of all (wake) particles with azimuthal velocities of greater than 0.8 times the sound speed, with panels for each of the 10, 20, 30, 40, and 50 M_J models.

drodynamics responsible for the periodic angular momentum accretion in the 50 M_J model. The right panel shows a time just after a pulsational shock has passed through the gas, when the velocity vectors have an outward radial velocity component (toward the upper left), except in the vicinity of the companion. The left panel shows the velocity field at a time about midway between shock passages, when most of the velocities have a radial infall component (toward the lower right).

In the left panel we see gas flowing around the inner side of the companion, and encountering a shock where the velocity vectors get smaller and turn. In the post-shock wake this material streams around and behind the companion, where it encounters a shock separating it from material flowing in from the outer side of the companion. The latter stream is turned aside. The vortex likely formed in this sense because gas coming around on this side encounters the wake and is shocked. The outer stream hits the wake at a glancing angle and is deflected. The inner stream finally spirals onto the companion in a counterclockwise sense.

In the right panel the situation is reversed. It is the

outer stream that impacts the wake, is shocked, and streams around and onto the companion in a clockwise sense. In this case, when the pulsational shock has just passed, the wake and its vortex structure is more compressed.

Shock passage moves and compresses the wake quite abruptly, accounting for the rapid drop in accreted angular momentum in the last plot of Figure 8. After that the radial flow slows and reverses, and it takes most of the cycle to reform the vortex of the left panel of Figure 9. This accounts for the relatively slow rise of angular momentum in the 50 M_J model.

In sum, the change in the nature of angular momentum accretion from quite random to nearly periodic is associated with the increasing role of accretion out of the more distant parts of the wake, and the formation of wake vortices with alternating senses of rotation. This is in contrast to the mass accretion, which is periodic in low mass models because of its immediate sensitivity to the passage of pulsational shocks.

As in the case of mass accretion, there are both similarities and differences in the angular momentum accretion of the X-ray binary flip-flop case and the present case. Like

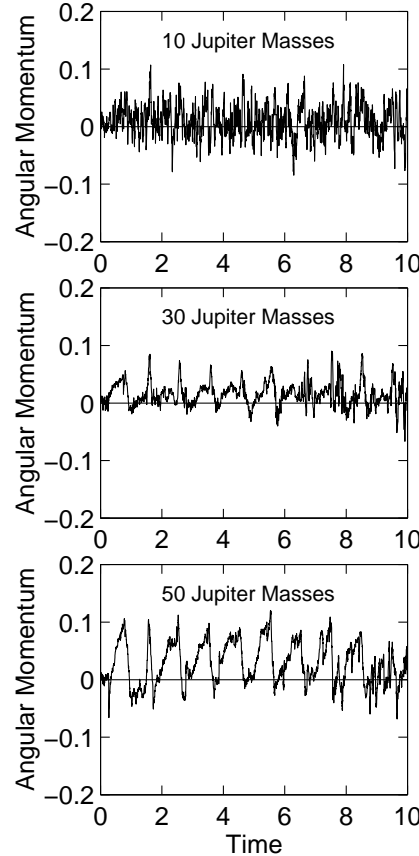


Figure 8. Comparison of the mean specific angular momentum relative to the companion versus time for the 10, 30, and 50 M_J models. The mean is computed for all particles accreting at that time. The y-axis is labelled in code units, i.e., $AU^2\ yr^{-1}$.

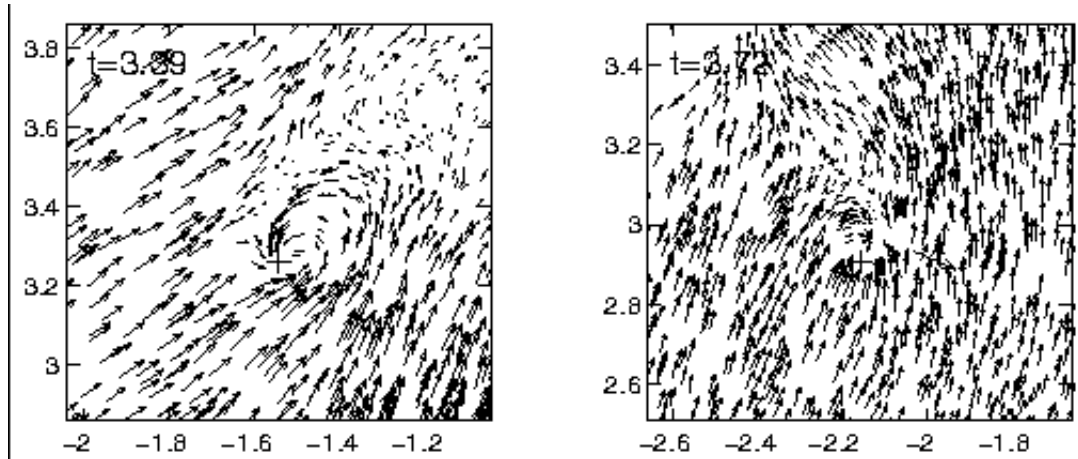


Figure 9. Particle velocity vectors relative to the companion (cross), in a small area around the companion in the 50 M_J model, at $t=3.39$ and 3.72 . Every fourth particle plotted.

the present case, the value of the accreted specific angular momentum is highly variable in the flip-flop models (e.g., Benensohn, Lamb, & Taam 1997, Ruffert 1997, 1999). The variations can be of comparable magnitude to those in the present case, and also include sign changes in the accreted angular momentum. The variations in the three-dimensional models of Ruffert (1997, 1999) are not as regular as the high mass cases shown in Figure 8, but the two-dimensional sim-

ulations of Benensohn, Lamb, & Taam (1997) are very similar. However, these flip-flop models are mostly adiabatic, and we recall that there is no flip-flop instability in the isothermal case.

4 OBSERVATIONAL CONSEQUENCES

In this section we consider the ramifications of the results of the previous section for observation. Before beginning we recall that the models above were focussed on a particular region of parameter space. Specifically, we considered stellar companions in the mass range of $10 - 50 M_J$, orbiting at a radius of $r = 4.0 \text{ AU}$ from an approximately $1.0 M_\odot$ Mira, a region in the extended stellar atmosphere where pulsational motions are still important. In the discussion below we will also compare the results above to those of Paper I, and note possible observational effects beyond this parameter range.

4.1 Optical Variability

In Willson & Struck (2001), in Paper I, and in Section 1 above we considered the possibility that accretion processes onto a companion might help explain the short time-scale optical variability in Miras studied by de Laverny, et al. (1998) in Hipparcos data. In this subsection we reconsider this issue in light of the new model results.

The models simulate the flow on the outer or accretion scale, and provide no direct information about the inner scale, near the companion. However, the properties of the captured material, like its time dependent angular momentum, allow us to infer a good deal about the behavior on the small scale.

Consider first the low mass companions where the accreted angular momentum varies relatively stochastically, with a low mean value. For example, in the case of a $10 M_J$ companion, the specific angular momentum is about $h = 0.02 \text{ AU}^2 \text{ yr}^{-1} = 1.4 \times 10^{17} \text{ cm}^2 \text{s}^{-1}$ (see Figure 8). If gas elements with this value of h settle into a circular accretion disc around the companion, without loss or gain of angular momentum, then the radius of that disc would be of about,

$$\frac{R}{R_J} = \left(\frac{h}{9.5 \times 10^{16}} \right)^2 \left(\frac{10 M_J}{M} \right)^{1/2}, \quad (4)$$

where R_J is the radius of Jupiter. In the example with a $10 M_J$ companion, and $h = 0.02 \text{ AU}^2 \text{ yr}^{-1}$, this equation yields $R = 2.3 R_J$. Thus, at the low end of the mass range considered above, the significant fraction of the accreted gas with specific angular momentum somewhat smaller than this value (or companion mass or radius somewhat larger) can fall directly onto the companion surface. The rest may be found in a small, and continually disturbed, accretion disc. (We note that such discs are much smaller than those of Mastrodemos & Morris (1998, 1999), whose stellar mass companions, located in steady outflows, accrete gas with higher values of the specific angular momentum.)

We discussed mass accretion rates in Section 3.2. With those rates, and if we assume that accreted particles hit the surface of a $30 M_J$ companion of radius about $1.0 R_J$ with about free-fall velocity, and that essentially all of their kinetic energy is converted into optical luminosity, then the magnitude of this luminosity is,

$$L = \frac{1}{2} \dot{M} v_{ff}^2 = 0.090 L_\odot \left(\frac{v_{ff}}{330 \text{ km/s}} \right)^2. \quad (5)$$

This value is for accretion bursts and is correspondingly

smaller for the low accretion rates between bursts. It also assumes an optimistic conversion of accretion energy to optical photons. On the other hand, it would be substantially increased for a somewhat more massive companion in the denser wind of a more evolved Mira. It would be reduced in the case of greater star/companion separations.

These results are in agreement with those of our earlier papers, where we found that there would probably not be sufficient energy in the mean accretion onto giant planets to produce optical flashes. We conjectured that gas with angular momentum of one sign might be accreted for about half a pulsation cycle, and stored in a disc. Then in the second half of the cycle a comparable mass of gas with angular momentum of opposite sign might rain down and flush the disc onto the companion. The large mass of stored gas could produce luminosities large enough to be observable at stellar minimum light.

In the case of X-ray binaries, this disc storage and flushing has long been considered as a possible explanation for the rapid changes in the luminosity and period of X-ray pulsars (Taam & Fryxell 1988). More recently, Benensohn, Lamb, & Taam (1997) estimated that in favorable cases, angular momentum accretion reversals could be responsible for abrupt spin changes in some X-ray pulsars.

Figure 8 suggests that for the lower companion masses there is no periodicity in the accreted angular momentum, so the simple storage mechanism will not work. Most of the time the accreted angular momentum has a positive sign, so most of the time some fraction of this material adds to the small disturbed disc mentioned above. Occasionally there are bursts of negative angular momentum accretion. If these bursts contain enough mass, or their angular momentum is sufficiently negative, then they might dump enough material onto the companion to produce an observable burst. In numerical models such random bursts are partially the product of noise resulting from small particle numbers. Turbulence or similar effects would likely generate them in the circumstellar environment.

Another possibility is that pressure from hot gas or magnetic fields could inhibit the flow to small scales until the accreted mass builds up to a critical level. The result could be a burst of quite large mass (and small angular momentum), like those in the model of Paper I. Interaction with a rotating magnetosphere could also add or subtract angular momentum to accretion disc gas. The study of such processes is beyond the scope of this paper.

In the case of large companion masses, Figure 4 shows larger mass accretion rates, and Figure 8 indicates quasi-periodic angular momentum accretion. Thus, the prospects for storage, followed by large bursts are much better. According to the estimate of Equation (1), with h values from Figure 8, the typical accretion disc radii are still small, of order a few times R_J . However, with the deeper gravitational potential, and higher mass accretion rates in bursts (accumulated in storage), the luminosity estimates from Equation (2) can exceed a solar luminosity. This is more than enough to give a detectable signal near minimum light in a large amplitude Mira, as noted in Willson & Struck (2001).

In fact, storage may not be required for observable optical effects at companion masses of about $50 M_J$ or higher. They might also be possible at fairly large radii where the ambient gas density is smaller and where pulsational shocks

are weak and there is essentially no radial motion. In this case the optical enhancement would be relatively constant, with no bursts, which would make it harder to distinguish from the Mira minimum luminosity. However, we would expect variations over the companion orbital period, as the companion is more or less hidden by the extended Mira atmosphere (unless its orbital plane coincided with the plane of the sky).

4.2 A Simple Model of the Inner Accretion Scale

To clarify the issues raised in the previous paragraphs it is worth extending the numerical results with a simple semi-analytical model of the inner accretion disc. We adopt the simplifying assumption that all particles accreted with negative angular momentum and a number of disc particles carrying an equal amount of positive angular momentum fall immediately onto the companion. After such events, the accretion disc is assumed to consist of all the remaining particles, with each carrying an equal part of the remaining cumulative angular momentum. With these approximations the model yields the amount of infall onto the planet and the angular momentum in the disc as functions of time.

Figure 10 shows some results of applying this simple model to data output at every timestep from the numerical hydrodynamical model, in the cases of the 10, 30, and 50 M_J models. In each case, the rapidly varying line shows the mass added to the disc versus time, which is negative if material falls onto the companion. The smoother solid curve shows the net specific angular momentum in the disc, and the dashed curve shows the net particle number in the disc. Comparison of these particle numbers with those of Figure 2 for the outer accretion shows that a significant fraction of the particles do fall onto the companion in this model.

The values of the specific angular momenta generally seem to settle to a limiting value in the three cases, though this is not entirely clear in the 10 M_J model. In the other two cases, this quantity first peaks, and then settles to a lower final value. Comparison shows that, in all cases, the final value for the model in Figure 10 is slightly higher than the mean in Figure 8. Presumably this is because the mean value of the accreted positive angular momentum is much greater than the mean negative value.

Finally, we can use Figure 10 and the first equality of Equation (5) to get another estimate of the magnitude of energetic outbursts from the planet. The typical timestep of the numerical model is about 1.5 days, and from Figure 10, the mass of infall onto the companion is typically a burst of about 30 particles in the 30 and 50 M_J models, respectively. These values translate into a mass accretion value of $4.6 \times 10^{17} \text{ g/s}$, and a luminosity of about $0.072 L_\odot$ for the 30 M_J model. The luminosity would be a few times greater for the 50 M_J model and mass infalls can also sometimes be a few times greater. Moreover, since the free-fall time at the mean disc radius is only a few hours, the numerical models may overestimate the infall time of a mass cluster, and thus, underestimate the luminosity. Luminosities of order $1.0 L_\odot$ seem quite possible. Note, in particular, that the estimates of Equation (2) are based on a relatively low Mira mass loss rate ($2 \times 10^{-7} M_\odot/\text{yr}$) and the corresponding mean ambient density.

As discussed above infall events come in clusters, so we would expect an outburst to be sustained for times of several days to several weeks, as seen in the Hipparcos data.

4.3 SiO Masers

In previous papers (Struck-Marcell 1988, Willson and Struck 2001, Paper I) we noted that the region of SiO maser emission in Miras with such emission coincides with the pulsating region of the extended atmosphere. Those works also discussed how the presence of a giant planet or brown dwarf companion at similar orbital radii could effect the SiO emission, e.g., with clumping due to turbulence in the wake to produce density enhancements needed for the masering, and with relatively strong local magnetic fields around the companion and in the wake to help explain the high polarizations of some maser stars.

The new models provide more detail on wake structure, especially in the case of high mass companions. On the other hand, information on the structure of clumps is limited, because that will depend on detailed cooling and heating processes not included in our isothermal equation of state. Despite this limitation, Figure 7 still shows the presence of substantial inhomogeneities in the wakes. The vortices in Figure 9 provide an even more striking example of inhomogeneous flow. The wake bounding shocks visible in Figure 9, combined with the AU length of the wakes in Figure 7, show that there are substantial shock surfaces. Wake and pulsational shocks are of comparable amplitude in the models above. Thus, the wake environment should be just as favorable as that of the pulsational shocks for exciting SiO molecules.

Moreover, the last three panels of Figure 1 show that the companion and the wake can noticeably ripple the outer edge of pulsational shocks, and perturb the gas behind that edge, over a large azimuthal angle. As a result, wakes may also enhance clumping behind pulsational shocks. Hartquist & Dyson (1997) have suggested that pulsational shocks are mediated by strong magnetic fields (of order 50 G), and that clumps result from the action of the Parker instability in those shocks. One obvious difference between the two models is that companion induced clumping occurs around an orbital ring, which could be highly flattened in some views. The Hartquist and Dyson clumping, like clumping in the pulsational shocks, would be spherically symmetric, in the absence of rotational flattening, and probably be seen as always circular, with limb brightening. The maser spots of *o Ceti* (Mira) appear to have a fairly flattened distribution, which could be a ring viewed edge-on (Phillips & Boboltz 2000).

The range of sizes in the wake and wake inhomogeneities in the substellar companion model (i.e., of order tenths of an AU up to a few AU) also seem in accord with VLBI observations of SiO maser spots. For example, maser spots subtending an angle of 3 milliarcseconds, near a Mira at a distance of about 300 pc, have a physical extent of about 1 AU. (These numbers derive from Kemball & Diamond (1997) study of TX Cam, but are also appropriate for *o Ceti*, see Phillips & Boboltz (2000).)

The shortest time-scales reported for variations in SiO maser line profiles are about 10-20 days (Pijpers, et al. 1994). This corresponds to a distance of a few hundredths of

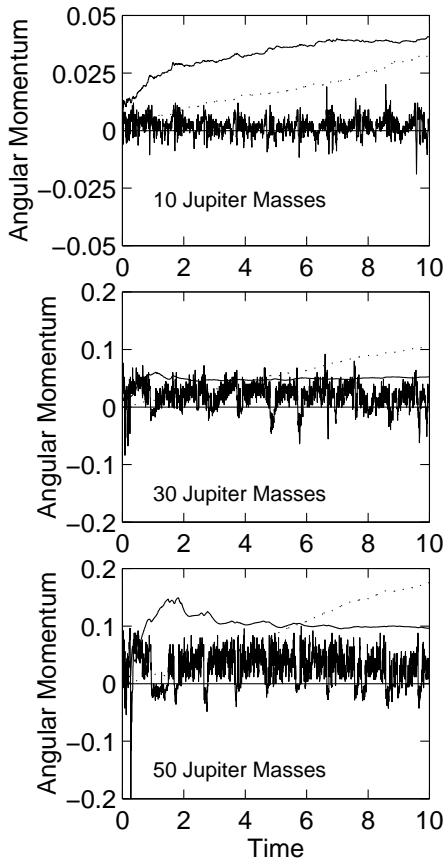


Figure 10. Comparison of properties of the semi-analytical inner disc model versus time for the 10, 30, and 50 M_J models. The rapidly varying solid curve in each panel shows the amount of mass added to the inner disc in units of 1000 particles. Positive values indicate particles added, while negative values indicate particles lost from the disc that fall onto the companion (see text). The dashed curve shows the net particle number in the disc in units of 10^5 particles. The slowly varying solid curve is the net specific angular momentum of the inner disc in dimensionless code units, but which has been multiplied by a factor of 2 in the bottom two plots for clarity.

an AU for a roughly sonic velocity of about 5.0 km/s, and still less than 0.1 AU for shocks propagating at 10 km/s. Thus, such rapid changes must be associated with quite small scale dynamical phenomena, such as a shock passage, collisions between small clumps, or interactions on the small scale near a companion. On the other hand, lifetimes of specific spectral features can range up to several hundred days, which would correspond to a sonic traversal distance of close to an AU. Such motions could include either traversal of a companion wake or the development of a clump in a hydro-magnetic instability.

4.4 More Speculative Possibilities

In this subsection we consider some more speculative possibilities for detecting planetary or brown dwarf companions to Miras. These include effects related to the presence of: 1) a hot corona around the companion, and 2) intermittent jets launched from the companion.

4.4.1 Coronae

We have described above how Mira wind material may fall onto the companion and an accretion disc with a typical radius of several times that of the companion radius, at about

free fall velocities. With the companion mass range considered in this paper, these velocities are of order 300 km/s. Collisions between gas elements with such relative velocities could generate gas temperatures of millions of Kelvins in at least a fraction of the gas. At the high densities of the companion surface, and even the accretion disc surface, cooling is probably very efficient. However, less dense gas in the atmospheres of the companion and the disc can be heated either in the collision or by absorbing the cooling radiation.

In Paper I we estimated that, if converted to ionizing photons, the accretion luminosity could ionize a sphere of radius of order $10 R_J$ around the companion (depending on many poorly known parameters). The pressure scale height of gas with a temperature of a few million degrees is also of order $10 R_J$. Thus, this material is deep within the capture radius of the companion, so any passing circumstellar gas will be captured, and will not sweep the corona out.

We would expect the coronal gas to be of quite low density relative to its surroundings. For example, we can require that its free cooling time be greater than about 1 yr., a typical time between accretion bursts or pulsational wave passages. Then with a high temperature cooling rate of about $2 \times 10^{-23} \text{ ergs cm}^3 \text{ s}^{-1}$ (e.g., Spitzer 1978), we find that the coronal density must be less than about 1000 cm^{-3} . Given this density and a volume corresponding to the radius above,

we find that the emission associated with coronal cooling is negligible ($< 10^{-17} L_\odot$). Generally, we expect that to obtain a detectable coronal emission measure would require a material density that is high enough to give a cooling time of much less than a year. Thus, while a corona is an interesting component of the companion region, is not directly observable. Most of the accretion energy will be emitted from transient hot spots on the disc and companion.

4.4.2 Magnetosphere and Coronal Wind

The companion may have a magnetic field, and magnetosphere, like that of Jupiter. If so, it would have an important effect on the corona and the accretion disc. First of all, we note that the magnetic pressure, given a surface field of about 3.0 G, would be of the order,

$$P_B = 3.6 \times 10^{-7} \left(\frac{B_{\text{surf}}}{3.0 \text{G}} \right)^2 \left(\frac{10R_J}{R} \right)^6 \text{ dyne cm}^{-2}, \quad (6)$$

at a distance R from the companion centre. This is generally comparable to or greater than the thermal pressure of a maximum density corona given by,

$$P_{\text{th}} \leq 6.2 \times 10^{-7} \left(\frac{n}{1000 \text{ cm}^{-3}} \right) \left(\frac{T}{3.0 \times 10^6 \text{ K}} \right). \quad (7)$$

When hot gas is created in accretion impacts it will begin to expand out into the corona, but it will also be constrained by the magnetic field.

If the companion and its magnetosphere are rotating like Jupiter, then the centrifugal force will be important, e.g., in driving a centrifugal wind. Soker & Rappaport (2000) and Soker (2002) have also discussed the formation of companion winds around AGB stars. However, the case they considered was that of a white dwarf or main sequence companion, which is able to spin up the Mira atmosphere, and induce strong Roche lobe accretion onto the companion. This induces a strong fast wind. The cases considered in this paper generally fail to meet Soker & Rappaport's condition for strong tidal interaction, though the most massive brown dwarfs orbiting within a few AU would be affected. Therefore we would not expect as strong a wind as described in their work.

Nonetheless, once the accretion disc builds up to a substantial mass, the environment around it may be quite similar to that around a magnetic protostar. The X-wind theory of Shu and collaborators (e.g., Shu et al. (1999) and references therein) may be applicable. However, the mass and energy in such a variable wind would be much less than in the protostellar case, so it seems unlikely that these effects would be directly observable.

5 SUMMARY AND CONCLUSIONS

In the models described above we have studied the interaction between the extended, pulsating atmosphere and wind of a Mira variable and a brown dwarf or giant planet companion. Our numerical models resolved the time-dependent bow shock and wake structure created by the companion. The outermost parts of the accretion onto the companion were also resolved. We obtained the following results concerning the gas flow.

1) The accretion rate scales roughly linearly (in two dimensions) with the companion mass. (See Fig. 3 and Section 3.2.)

2) The equation of state, or more precisely the value of the exponent γ of the adopted barotropic equation, has little effect on the accretion rate. Naively, this is because accretion is the result of gravitational capture under conditions where the thermal pressure is small.

3) One of the most interesting results above is the transition from periodic to chaotic mass accretion, and from chaotic to periodic angular momentum accretion as the companion mass is increased through the range considered in this paper ($10 - 50 M_J$). (See Figs. 4 and 8, and Sections 3.3 and 3.4.)

4) The wakes grow substantially as the companion mass is increased through this range. Wake structure, and in particular, clumping could have an important effect on SiO maser emission, which derives from the same region. (See Fig. 6 and Section 4.3).

While we do not resolve the flow on the inner scale ($R < 200 R_J$), we did monitor the mass and angular momentum accreting into this region. With these data and a few simplifying assumptions, we examined the properties of a simple semi-analytic model for this flow (Section 4.2). Using this model we obtained the following additional results for flow on the inner scale.

5) The effective boundary conditions between the inner and outer scales are important. In Paper I we adopted a boundary condition equivalent to the assumption that it was difficult for accreting gas to penetrate to the inner scale. This leads to strong bursts of accretion. This case requires coronal or magnetospheric pressure to be strong enough to resist the infalling gas. Estimates of the corona derived from our semi-analytic model, and of magnetospheres comparable to that of Jupiter, suggest that that would not be the case with companions like those studied in this paper.

6) The semi-analytic model suggests that an accretion disc would form around the companion on a scale of order a few companion radii (see Section 4.4).

7) The pattern of angular momentum accretion (positive and negative) suggests that accretion bursts are likely. They may be strong enough to generate observable effects in the optical (see Section 4.1).

8) Energy dissipation from the impact of free-falling gas elements on the companion and the accretion disc may generate a thin hot corona around the companion, and possibly a coronal wind (see Section 4.4). It is unlikely that these would be directly observable.

In sum, the situation studied in this paper is a previously unstudied type of close binary interaction. This interaction is different from that of the more well known symbiotic and cataclysmic type binaries in several respects. First of all, the close companion in those systems is generally a more massive white dwarf or M dwarf, and the interaction may involve mass transfer via Roche lobe overflow, or interacting winds, rather than direct accretion out of a Mira wind. A second aspect of the present study is the inclusion of a radially oscillating environment, which we found has profound effects on the accretion process.

The oscillating environment has not generally been considered in models of other types of close AGB binaries. However, as Mastrodemos & Morris (1998) and Soker (2002)

have pointed out, a close massive companion would exert significant tidal forces on the Mira atmosphere. Moreover, the Mira would have a significant motion around the centre of mass. These and other relatively energetic phenomena make it unlikely that such systems would be classified as ordinary Miras. Such cases deserve further study.

Several other issues raised above also merit further study. The first is the thermohydrodynamics of the inner scale. Fully self-consistent numerical modeling with heating and cooling and magnetic fields included would be very interesting, if not entirely feasible at present. Including heating, cooling and magnetic effects in the wake flow would also be very interesting, especially to see the impact of these processes on SiO maser emission. However, the most urgent need is for more observational constraints on the models. The models above provide a number of observationally testable predictions. The observations published to date provide intriguing hints, but are not sufficient to provide strong evidence for the existence of such systems or strong tests of the models.

ACKNOWLEDGMENTS

We are grateful to G. H. Bowen for many helpful conversations on Miras, and to an anonymous referee for numerous helpful suggestions. This research has made extensive use of the NASA IPAC Extragalactic Database (NED).

REFERENCES

Balick, B., Wilson, J., & Hajian, A. R. 2001, AJ, 121, 354
 Benenohn, J. S., Lamb, D. Q., & Taam, R. E. 1997, ApJ, 478, 723
 Bondi, H., & Hoyle, F. 1944, MNRAS, 104, 273
 Bowen, G. H. 1988, ApJ, 329, 299
 Cowie, L. L. 1977, MNRAS, 180, 491
 de Laverny, P., Mennessier, M. O., Mignard, F., & Mattei, J. A. 1998, A&A, 330, 169
 Foglizzo, T., & Ruffert, M. 1997, A&A, 320, 342
 Foglizzo, T., & Ruffert, M. 1999, A&A, 347, 901
 Frink, S., Mitchell, D. S., Quirrenbach, A., Fischer, D. A., Marcy, G. W., & Butler, R. P. 2002, ApJ, 576, 478
 Fryxell, B. A., Taam, R. E., & McMillan, S. L. W. 1987, ApJ, 315, 536
 Fryxell, B. A., & Taam, R. E. 1988, ApJ, 335, 862
 Gail, H.-P., & Sedlmayr, E. 1999, A&A, 347, 594
 Hartquist, T. W., & Dyson, J. E. 1997, A&A, 319, 589
 Hill, S. J., & Willson, L. A. 1979, ApJ, 229, 1029
 Ho, C., Taam, R. E., Fryxell, B. A., Matsuda, T., & Koide, H. 1989, MNRAS, 238, 144
 Hoyle, F., & Lyttleton, R. A. 1939, Proc. Cambridge Phil. Soc. 35, 405
 Humphreys, E. M. L., Gray, M. D., Yates, J. A., Field, D., Bowen, G. H., & Diamond, P. J. 2002, A&A, 386, 256
 Ishii, T., Matsuda, T., Shima, E., Livio, M., Anzer, U., & Boerner, G. 1993, ApJ, 404, 706
 Kemball, A. C., & Diamond, P. J. 1997, ApJ, 481, L111
 Liu, M. C., Fischer, D., Graham, J. R., Lloyd, J. P., Marcy, G. W., Butler, R. P. 2002, ApJ, 571, 519
 Livio, M., & Soker, N. 2002, ApJ, 571, L161
 Livio, M., Soker, N., Matsuda, T., & Anzer, U. 1991, MNRAS, 253, 633
 Lucas, P. W., & Roche, P. F. 2000, MNRAS, 314, 858
 Marcy, G. W., & Butler, R. P. 2000, PASP, 112, 137
 Marcy, G. W., Butler, R. P., Vogt, S. S., Liu, M. C., Laughlin, G., Apps, K., Graham, J. R., Lloyd, J., Luhman, K. L., & Jayawardhana, R. 2001, ApJ, 555, 418
 Mastrodemos, N., & Morris, M. 1998, ApJ, 497, 303
 Mastrodemos, N., & Morris, M. 1999, ApJ, 523, 357
 Phillips, R. B., & Boboltz, D. A. 2000, AJ, 119, 3015
 Pijpers, F. P., Pardo, J. R., & Bujarrabal, V. 1994, A&A, 286, 501
 Pogorelov, N. V., Ohsugi, Y., & Matsuda, T. 2000, MNRAS, 313, 198
 Reid, I. N., et al. 1999 ApJ, 521, 613
 Ruffert, M. 1994, A&AS, 106, 505
 Ruffert, M. 1995, A&AS, 113, 133
 Ruffert, M. 1997, A&A, 317, 793
 Ruffert, M. 1999, A&A, 346, 861
 Ruffert, M., & Arnett, D. 1994, ApJ, 427, 351
 Ruffert, M., & Anzer, U. 1995, A&A, 295, 108
 Shapiro, S. L., & Teukolsky, S. A. 1983, *Black Holes, White Dwarfs, and Neutron Stars: The Physics of Compact Objects*, Wiley, New York, Sec. 14.3
 Shu, F. H., Allen, A., Shang, H., Ostriker, E. C., & Li, Z.-Y. 1999, in C. J. Lada & N. D. Kylafis, eds. *The Origin of Stars and Planetary Systems*. Kluwer, Amsterdam, p. 219
 Soker, N. 1991, ApJ, 376, 750
 Soker, N. 1996a, ApJ, 460, L53
 Soker, N. 1996b, ApJ, 468, 774
 Soker, N. 2002, ApJ, 568, 726
 Soker, N., & Rappaport, S. 2000, ApJ, 538, 241
 Soker, N., & Rappaport, S. 2001, ApJ, 557, 256
 Spitzer, L. 1978, *Physical Processes in the Interstellar Medium*, Wiley, New York
 Struck, C. 1997, ApJS, 113, 269
 Struck, C., Cohenim, B. E., & Willson, L. A. 2002, ApJ, 572, L83 (Paper I)
 Struck-Marcell, C. 1988, ApJ, 330, 986
 Taam, R. E., & Fryxell, B. A. 1988, ApJ, 327, L73
 Taam, R. E., & Fryxell, B. A. 1989, ApJ, 339, 297
 Taam, R. E., Fu, A., & Fryxell, B. A. 1991, ApJ, 371, 696
 Willson, L. A. 2000, ARAA, 38, 573
 Willson, L. A., & Struck, C. 2001, JAAVSO, 30, 23
 Zapatero Osorio, M. R., Bejar, V. J. S., Martin, E. L., Rebolo, R., Barrado y Navascues, D., Bailer-Jones, C. A. L., & Mundt, R. 2000, Science, 290, 103